Journal of Marine Research, 47, 55–79, 1989

Eddy momentum and heat fluxes and their effects on the circulation of the equatorial Pacific Ocean

by Harry L. Bryden[1] and Esther C. Brady[1]

ABSTRACT

Eddy momentum and heat fluxes are estimated from three-dimensional arrays of long time-series current meter measurements in the equatorial Pacific near 152W and 110W during 1979 to 1981. Eddies transport eastward momentum away from the equator above the core of the Equatorial Undercurrent; they transport eastward momentum toward the equator below the Undercurrent core. The vertical integral of the eddy momentum flux divergence is equivalent to a westward wind stress of 0.16 dyne cm^{-2}. Eddies transport heat toward the equator at all depths down to 250 m. At 100 m depth and below, the eddy heat flux convergences are remarkably similar at 152W and 110W. Above 100 m, the heat flux convergence at 110W is much larger than that at 152W. The vertical integral of the average eddy heat flux convergence between 152W and 110W is equivalent to a heating of the equatorial region at a rate of 245 W m^{-2}. Lateral eddy viscosities and diffusivities are of order 0.5 to 5 $\times$ 10^7 cm^2 s^{-1}, similar to those generally used in numerical models. Eddy coefficients, however, are positive only above the core of the Equatorial Undercurrent and are consistently negative below the Undercurrent core. Fluctuations with periods between 32 and 13 days and centered at 21-day period contribute the bulk of the eddy heat and momentum fluxes.

I. Introduction

The equatorial Pacific ocean is a region of great natural variability. While interannual El Nino events (Halpern, 1987) dominate popular ideas of equatorial variability, fluctuations of shorter time scale are also energetic. There is a large seasonal signal in the equatorial circulation (Wyrtki, 1974). Kelvin waves regularly traverse eastward along the equator (Eriksen *et al.*, 1983). The fascinatingly periodic 21-day oscillations stand out in all upper ocean time series measurements (Philander *et al.*, 1985). Such fluctuations may be important for the dynamics and thermodynamics of the large-scale equatorial circulation and parameterization of their heat and momentum fluxes may be essential for the development of realistic models.

Hansen and Paul (1984) used satellite-tracked drifting buoy trajectories to estimate surprisingly large lateral mixing of momentum and heat in the surface layers of the equatorial Pacific. They found an eddy momentum flux divergence away from the equator equivalent over an assumed mixed layer of 50 m depth to a westward stress of

1. Woods Hole Oceanographic Institution, Woods Hole, Massachusetts, 02543, U.S.A.

0.3 dyne cm^{-2} and an eddy heat flux convergence equivalent to a heating of the equatorial mixed layer of 180 W m^{-2}. Such momentum flux divergence is comparable to the typical westward wind stresses of order 0.5 dyne cm^{-2} which drive the equatorial circulation, and their eddy heat flux convergence is larger than the typical atmosphere heating of the equatorial ocean of order 75W m^{-2}.

It is common in numerical models of equatorial circulation to parameterize lateral mixing effects with constant values of eddy viscosity and eddy diffusivity of order 1×10^7 cm^2 s^{-1}. For the observed meridional curvature in zonal velocity of 10^{-12} cm^{-1} s^{-1} associated with the Equatorial Undercurrent, lateral mixing of momentum must be equivalent in such numerical models to a deceleration of the eastward flow of order 0.1 cm^2 s^{-2} (dyne cm^{-2}) or 20% of the mean westward wind stress. Similarly for the observed curvature in temperature of 10^{-14}°C cm^{-2} associated with the Undercurrent, lateral mixing of heat must be equivalent to a heating of the equatorial region above the core of the Undercurrent of order 40 W m^{-2}, or 50% of the mean atmospheric heating of the equatorial zone. Since such lateral mixing must make a substantial contribution to the dynamics and thermodynamics of equatorial models, it seems worthwhile to quantify lateral mixing effects directly from equatorial measurements.

Because Hansen and Paul's (1984) estimates are restricted to the surface layer sampled by the drifting buoys and because of the limited amount of drifter data which allowed only an average of 45 buoy days of data in each of the 0.5° latitude bins, it was decided to estimate eddy fluxes of momentum and heat from the arrays of moored current meter measurements made near 152W and 110W during 1979–81. These measurements generally extend down to 250 m depth, so that the vertical profile of eddy fluxes and their divergences can be determined. The duration of the moored time series also provides more reliable statistics on the eddy fluxes. From these estimates of eddy fluxes, it is of interest to determine: (1) whether the eddy momentum and heat flux divergences contribute substantially to the zonal momentum and heat budgets in the equatorial Pacific; (2) whether the effects of these eddy fluxes are adequately parameterized in models of equatorial circulation which use constant eddy viscosity and diffusivity; and (3) what time-scale processes contribute the bulk of the observed eddy momentum and heat fluxes. The goal of this work is to answer these questions from existing current meter measurements.

2. Data and methods

To investigate the effect of temporal fluctuations on the mean circulation of the equatorial Pacific, eddy fluxes of momentum and heat are estimated from the long-term current meter array measurements near 152W and 110W. The recent development of realistic models of equatorial circulation has somewhat overshadowed the analysis of actual measurements of the circulation. The remarkably long time series measurements, which have continued since 1979 at 110W (Halpern, 1987), offer an opportunity for extensive model comparisons and for direct determination of the

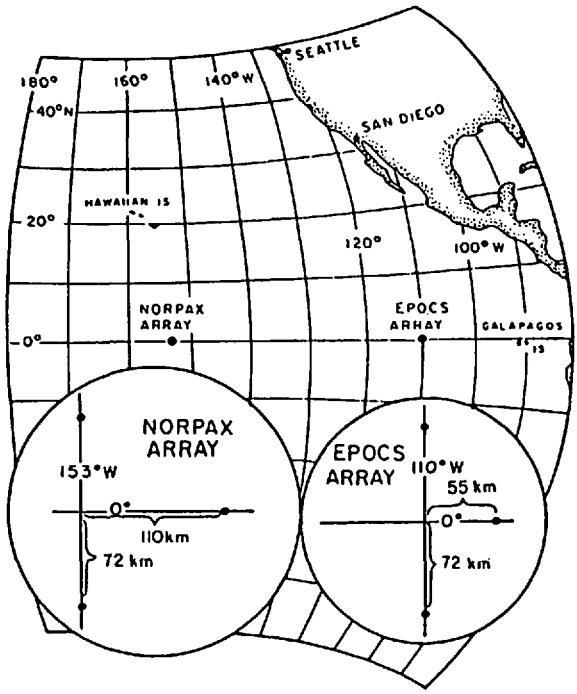

Figure 1. Three-dimensional arrays of moored current meter measurements in the equatorial Pacific during 1979 to 1981 (Knox and Halpern, 1982).

mean circulation and its temporal variability. Here, the effects of fluctuations on the time-averaged equatorial momentum and heat balances are estimated.

Because it is the divergence of eddy momentum and heat fluxes which is dynamically and thermodynamically important, the data used here consist of all three-dimensional arrays near 152W and 110W: that is, all arrays with moorings north or south of the equator as well as on the equator (Fig. 1). At 152W, the NORPAX arrays deployed for 15 months from April 1979 to June 1980 have been described by Knox and Halpern (1982). At 110W, the EPOCS three-dimensional arrays were deployed from January 1979 to October 1981. Each array consisted of a triangle of moorings, north and south of the equator at a latitude of about 40′ and an equatorial mooring displaced to the east. Each array was deployed for a period of 3 to 6 months so there were 3 settings of the NORPAX arrays and 6 settings of the EPOCS arrays. Each mooring had current meters also measuring temperature at depths of 15 or 20 m, 50 m, 100 m, 150 m and 250 m. The EPOCS moorings generally had additional current meters at 75 m and 200 m depths.

Each current meter record was put through a low-pass filter to obtain essentially daily-averaged values of east velocity, u, north velocity, v, and temperature, T. Means, variances and convariance for u, v, and T were then calculated. Overall means

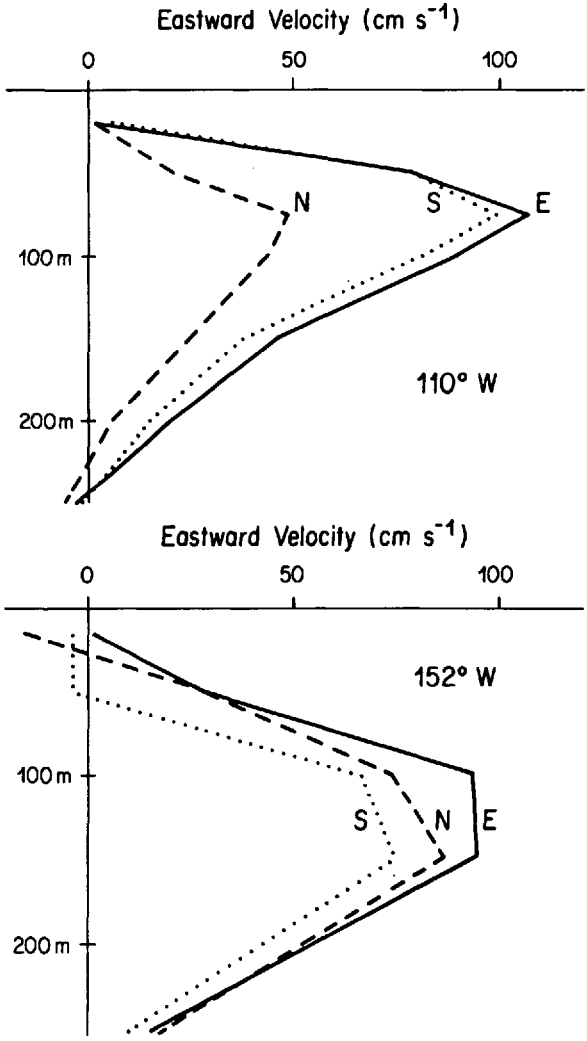

Figure 2. Time-averaged zonal velocity profiles at 110W and 152W in the equatorial Pacific. N denotes the north mooring, E the equatorial mooring and S the south mooring at each longitude.

$(\overline{u}, \overline{v}, \overline{T})$, variances $(\overline{u'^2}, \overline{v'^2}, \overline{T'^2})$ and covariances $(\overline{u'v'}, \overline{u'T'}, \overline{v'T'})$ at each site were calculated taking into account the duration of each record. Due to various instrument and mooring malfunctions, the time series near 152W vary in duration from 208 days to 389 days and near 110W from 381 days to 708 days.

The time-averaged zonal velocity profiles at 152W and 110W exhibit the subsurface maximum eastward velocity associated with the Equatorial Undercurrent (Fig. 2). The core of the Undercurrent is clearly deeper at 152W than 110W as noted by Halpern

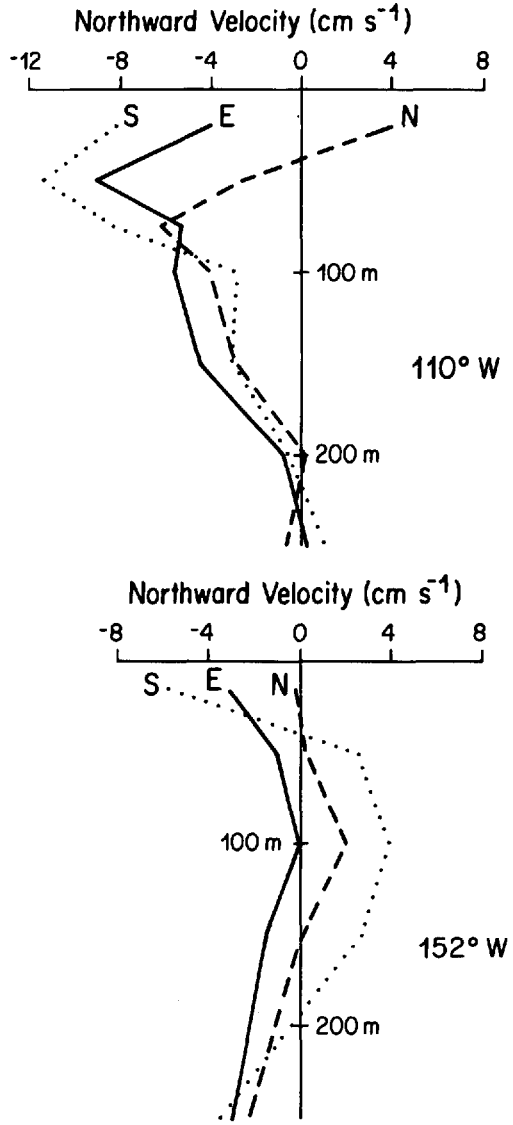

Figure 3. Time-averaged meridional velocity profiles at 110W and 152W in the equatorial Pacific.

(1980). From Bryden and Brady's (1985) diagnostic model of equatorial Pacific circulation, which is based on the annual-averaged geostrophic and wind-driven flows across the boundaries of the equatorial Pacific region between 150W and 110W and 5N and 5S during the period 1979 to 1981, the maximum Undercurrent velocity at 150W is at 120 m depth while at 110W it is at 60 m. The time-averaged meridional velocities (Fig. 3) are divergent in the upper waters as anticipated for a westward wind

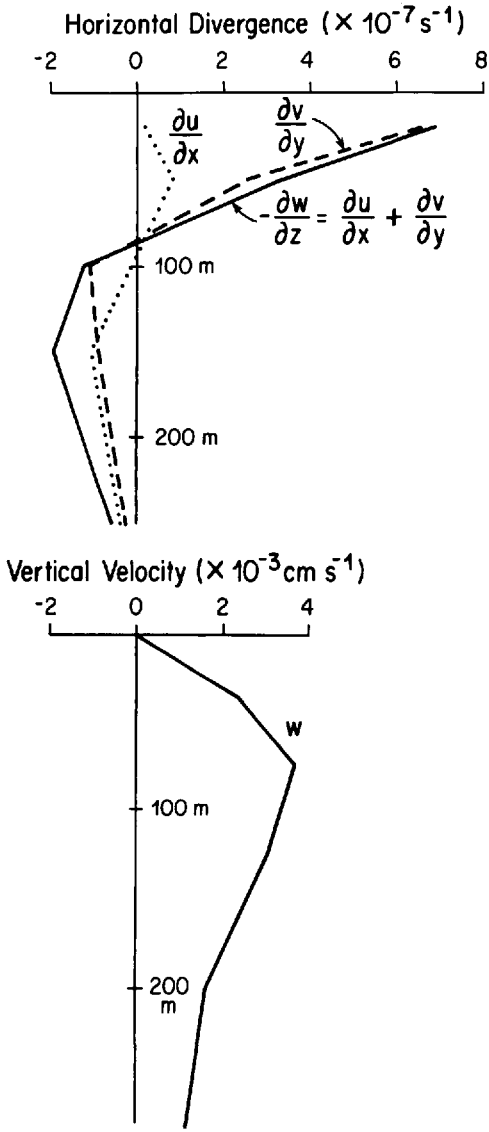

Figure 4 (a) Horizontal divergence of the time-averaged velocity field between 152W and 110W, 0°40′N and 0°40′S; (b) Vertical velocity profile derived by integrating the horizontal divergence vertically down from $w = 0$ at the surface.

stress and convergent in the deeper water. The zonal convergence below 100 m depth contributes substantially to the total deep horizontal convergence of the velocity field and thus to the profile of vertical velocity derived by vertically integrating the horizontal convergence (Fig. 4).

Errors in the time-averaged horizontal velocities are determined by calculating the standard error of the temporal fluctuations. The square root of the variance divided by

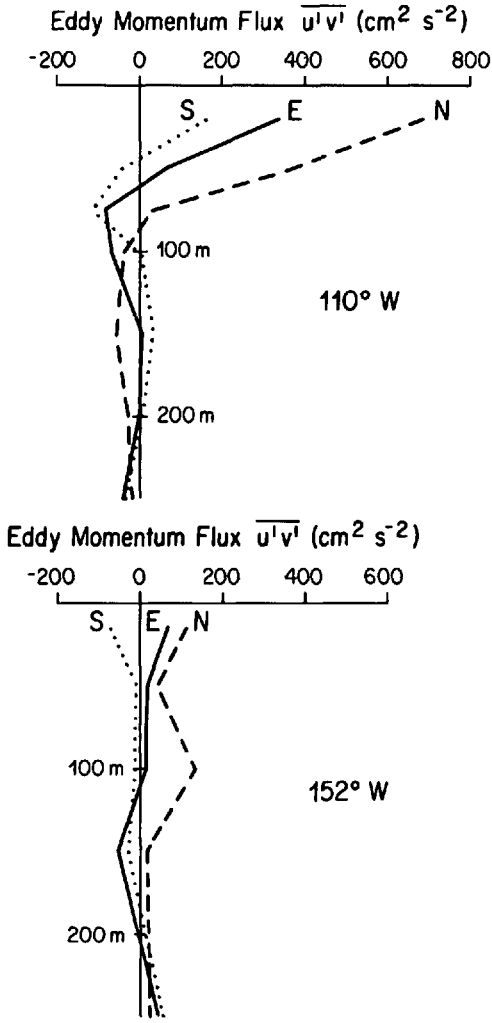

Figure 5. Eddy momentum flux profiles at 110W and 152W in the equatorial Pacific.

the number of integral time scales contained in each data record defines the standard error. Integral time scales are typically 17 days for the zonal velocity fluctuations and 7 days for the meridional velocity fluctuations. Zonal velocities then have standard errors increasing from about 3 cm s^{-1} at 250 m to 10 cm s^{-1} at and above the depth of the Undercurrent. Meridional velocities have standard errors increasing from 1.5 cm s^{-1} at deeper levels to 3.5 cm s^{-1} at the surface. Carrying these errors through the horizontal convergence calculation suggests that the maximum vertical velocity at 75 m depth of 3.65×10^{-3} cm s^{-1} has an error of 1.2×10^{-3} cm s^{-1}.

Eddy momentum fluxes, $\overline{u'v'}$, are large and positive in the upper 50 m at 110W and are smaller but more symmetric about the equator at 152W (Fig. 5). At both

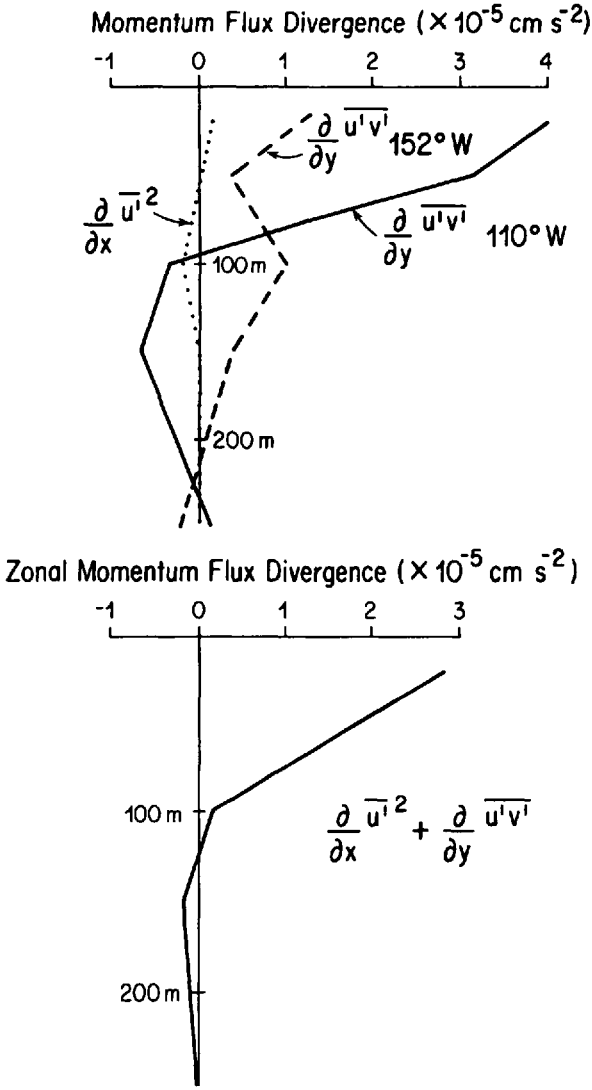

Figure 6. (a) Meridional divergence of the eddy momentum flux at 152W and 110W and zonal divergence of zonal momentum flux between 152W and 110W; (b) Horizontal divergence of the zonal eddy momentum fluxes between 152W and 110W, 0°40′N and 0°40′S.

longitudes, the equatorial momentum flux values generally lie between the northern and southen values; such consistency indicates that the meridional gradient of the eddy momentum flux, $\partial/\partial y\ \overline{u'v'}$, can be estimated reliably from the difference between the northern and southern values at each longitude (Fig. 6).

Uncertainties in the eddy momentum fluxes are estimated from the zonal and meridional velocity variances, $\overline{u'^2}$ and v'^2, and from the number of integral time scales,

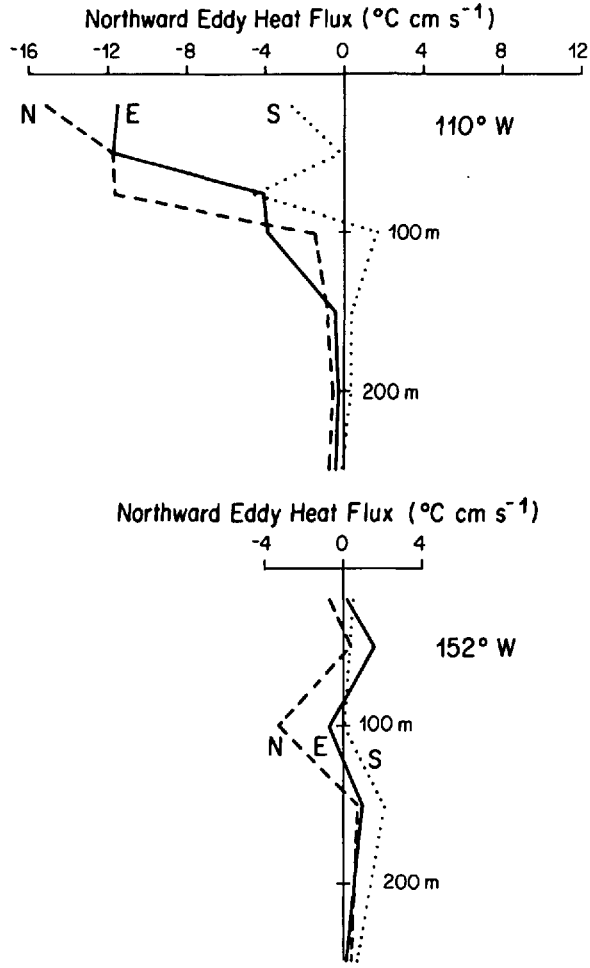

Figure 7. Meridional eddy heat flux profiles at 110W and 152W in the equatorial Pacific.

τ, contained in the time series of length t at each site:

$$\delta(\overline{u'v'}) = \sqrt{\overline{u'^2}\,\overline{v'^2}\left(\frac{t}{\tau}\right)}.$$

The integral time scales for second moments are estimated by integrating the product of the zonal and meridional velocity autocorrelation functions over lag time (Davis, 1976). The eddy momentum flux integral time scales vary from 5 to 9 days at 152W and from 4 to 7 days at 110W. Eddy momentum fluxes which are significantly different from zero at 95% confidence level are at 250 m depth on the southern mooring at 152W and at 20 m depth on the equatorial mooring and at 20 m, 50 m, and 150 m

depths on the northern mooring at 110W. Meridional gradients of the eddy momentum flux are significantly different from zero at 20 m, 50 m and 150 m depths at 110W.

Meridional eddy heat fluxes are large and generally directed southward at 110W and are smaller at 152W (Fig. 7). Again, the equatorial heat fluxes generally lie between the northern and southern heat fluxes indicating that meridional gradients, $\partial/\partial y\ \overline{v'T'}$, can be reliably estimated from the difference between northern and southern values (Fig. 8). Integral time scales for the heat fluxes are estimated by integrating the product of the meridional velocity and temperature autocorrelation functions over time lag. Such integral time scales vary only from 4 to 6 days at both 152W and 110W. Meridional eddy heat fluxes which are significantly different from zero at 95% confidence level are at 20 m 50 m, 75 m, 150 m and 200 m depths on the northern mooring and at 20 m, 50 m and 100 m depths on the equatorial mooring at 110W. Meridional gradients of the eddy heat flux are significantly different from zero at 20 m and 100 m depths at 110W.

3. Results

At both 152W and 110W, the eddy momentum fluxes are divergent above the core of the Undercurrent (Fig. 6). Just below the core, at 150 m depth at 152W and 75 m at 110W, the eddy momentum fluxes remain divergent. But deeper below the core, the eddy momentum fluxes become convergent. Thus, at and above the Undercurrent core, eddies transport eastward momentum away from the equator acting to decelerate the eastward flowing Undercurrent. Below the Undercurrent core, eddies transport eastward momentum toward the equator serving to accelerate the deeper portions of the Undercurrent. The vertical integral of the meridional divergence of the eddy momentum fluxes over the upper 275 m is equivalent to a westward wind stress of 0.12 dyne cm^{-2} at 152W and 0.21 dyne cm^{-2} at 110W. Errors in these vertical integral are estimated to be 0.08 dyne cm^{-2} at 152W and 0.07 dyne cm^{-2} at 110W. Calculating the horizontal divergence of the eddy momentum fluxes $\partial/\partial x\ \overline{u'^2} + \partial/\partial y\ \overline{u'v'}$, from the current meter measurements over the region 152W to 110W, 0°40'N to 0°40'S indicates that the eddy fluxes act overall to decelerate the eastward flow by 0.16 ± 0.05 dyne cm^{-2} in the zonal momentum balance. Such deceleration compares reasonably well with the deceleration of 0.11 dyne cm^{-2} inferred as a residual by Bryden and Brady (1985) for the eddy effects in their diagnostic model for the zonal momentum balance of the large-scale, time-averaged circulation.

At both 152W and 110W, the meridional eddy heat fluxes are convergent from the surface layer down to 250 m depth (Fig. 8). The heat flux convergence is larger above 100 m at 110W than at 152W, but at 100 m depth and below the heat flux convergences are remarkably similar at the two longitudes. Thus, eddies transport heat toward the equator at all depths down to 250 m. The vertical integral of the meridional eddy heat flux convergence down to 275 m depth is equivalent to a heating of the equatorial region of 95 W m^{-2} at 152W and 380 W m^{-2} at 110W. Errors in these

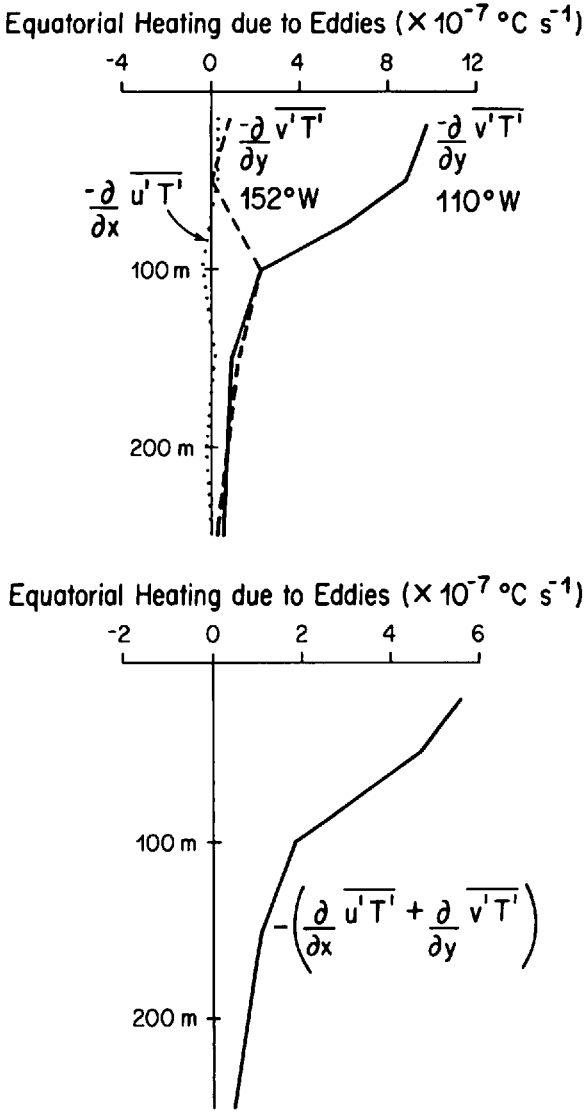

Figure 8. (a) Meridional eddy heat flux convergence at 152W and 110W and zonal eddy heat flux convergence between 152W and 110W; (b) Horizontal convergence of the eddy heat fluxes between 152W and 110W 0°40′N and 0°40′S.

vertical integrals are estimated to be 100 W m^{-2} at 152W and 135W m^{-2} at 110W. The horizontal divergence of the eddy heat fluxes, $\partial/\partial x\ \overline{u'T'} + \partial/\partial y\ \overline{v'T'}$, averaged over the region 152W to 110W 0° 40′ N to 0° 40′ S then acts overall to heat the equatorial waters at a rate of 245 ± 84 W m^{-2}. Bryden and Brady (1985) did not really infer an eddy heat flux contribution in their diagnostic model. Their model circulation

Table 1. Eddy viscosity.

Depth (m)	$\bar{u}_{yy}$ ($\times 10^{-13}$ cm^{-1} s^{-1})	$(\partial/\partial_y)\overline{u'v'}$ ($\times 10^{-5}$ cm s^{-2})	$A = -(\partial/\partial_y)\overline{u'v'}/\bar{u}_{yy}$ ($\times 10^{7}$ cm^2 s^{-1})	
15	−3.8	1.3	3.4	
50	−5.2	0.4	0.7	
100	−8.4	1.0	1.2	152W
150	−4.9	0.4	0.8	
250	−0.6	−0.2	−3.6	
20	0.9	4.0	−43.0	
50	−14.0	3.1	2.2	
75	−16.1	1.2	0.8	
100	−12.9	−0.3	−0.3	110W
150	−6.9	−0.7	−1.0	
200	−4.6	−0.3	−0.6	
250	−0.3	0.1	4.3	

required a net heating of only 25 W m^{-2}, all of which could be accounted for by heat gain from the atmosphere, of which typical values range between 50 to 85 W m^{-2}. Clearly, the eddy heat flux convergence at the equator makes a significant contribution to the equatorial heat budget, since it is a factor of 3 or 4 larger than the air-sea heat exchange.

Parameterization of these eddy momentum and heat fluxes by coefficients of eddy viscosity and eddy diffusivity can be studied by dividing the meridional curvature of zonal velocity and of temperature at each depth by the meridional divergence of eddy momentum flux and of eddy heat flux (Tables 1 and 2). The calculated eddy coefficients have a magnitude of order 10^7 cm^2 s^{-1}, similar to those used in models, but the eddy coefficients are positive only at and above the core of the Equatorial Undercurrent. Below the core both the effective eddy viscosity and eddy diffusivity are negative at both 152W and 110W. The existence of both positive and negative eddy viscosities has already been noted in the NORPAX measurement by Lukas (1987). In terms of the meridional eddy flux divergences discussed above, such negative eddy coefficients should be expected. For eddy viscosity calculations, the meridional curvature in zonal velocity is essentially negative everywhere in the upper 250 m while the eddy momentum flux divergence is positive above the Undercurrent core and negative below the core. For eddy diffusivity calculations, the eddy heat fluxes are convergent at all depths down to 250 m but the meridional curvature in temperature switches from positive to negative at the Undercurrent core as expected for a geostrophic Undercurrent with doming isotherms above the core and bowling isotherms below.

The calculated eddy viscosity coefficients vary in magnitude only from 0.3 to 3 $\times$ 10^7 s^{-1}, excluding the values of meridional curvature in zonal velocity less than 1 $\times$ 10^{-13} cm^{-1} s^{-1} which may be unreliable. Similarly, the eddy diffusivities generally vary

Table 2. Eddy diffusivity.

Depth (m)	$\overline{T}_{yy}$ ($\times 10^{-14}$°C cm^{-2})	$(\partial/\partial_y)\overline{v'T'}$ ($\times 10^{-7}$°C s^{-1})	$K = -(\partial/\partial_y)\overline{v'T'}/\overline{T}_{yy}$ ($\times 10^{7}$ cm^2 s^{-1})	
15	0.6	−0.8	1.4	
50	0.8	−0.01	0.01	
100	2.6	−2.2	0.9	152W
150	−1.0	−1.2	−1.3	
250	−1.3	−0.5	−0.4	
20	1.6	−9.7	6.0	
50	4.2	−8.8	2.1	
75	−1.2	−6.1	−5.2	
100	−0.5	−2.3	−4.8	110W
150	−0.8	−0.9	−1.1	
200	−0.5	−0.7	−1.3	
250	−1.1	−0.5	−0.5	

in magnitude from 0.5 to 5 × 10^7 cm^2 s^{-1}, although a very small diffusivity is estimated at 50 m depth at 152W where the meridional heat flux divergence seems abnormally small. Overall, the most notable feature of these eddy coefficients is that they are consistently positive at and above the core of the Undercurrent and consistently negative below the core.

To determine what time-scale processes give rise to the eddy momentum and heat fluxes and their divergences in the surface waters, cospectra between u and v and between v and T are calculated for the 20 m record on the north mooring at 110W where both the northward eddy flux of eastward momentum and the southward eddy heat flux are large and statistically significant. Cospectra for three 128-day pieces are averaged and plotted in a covariance-preserving format (Fig. 9). The positive eddy momentum flux and negative (southward) eddy heat flux are clearly the result of fluctuations in the frequency band with periods between 32 and 13 days. In each cospectrum, the maximum covariance occurs at 21.3 day period which strongly suggests that the eddy momentum and heat fluxes are associated with the energetic 21-day oscillations in the equatorial Pacific (Halpern *et al.*, 1988).

4. Discussion

One motivation for undertaking this study was to determine whether the substantial eddy momentum and heat fluxes calculated from drifting buoy trajectories in the region between 95W and 130W by Hansen and Paul (1984) would be confirmed by analysis of long-term current meter measurements. Their eddy heat fluxes, $\overline{v'T'}$, near the equator are similar in magnitude and direction to the current meter values of 110W at 20 m depth. Their momentum fluxes, $\overline{u'v'}$ however, are a factor of two larger near the equator, exhibiting a maximum of order 1500 cm^2 s^{-2} versus the current meter

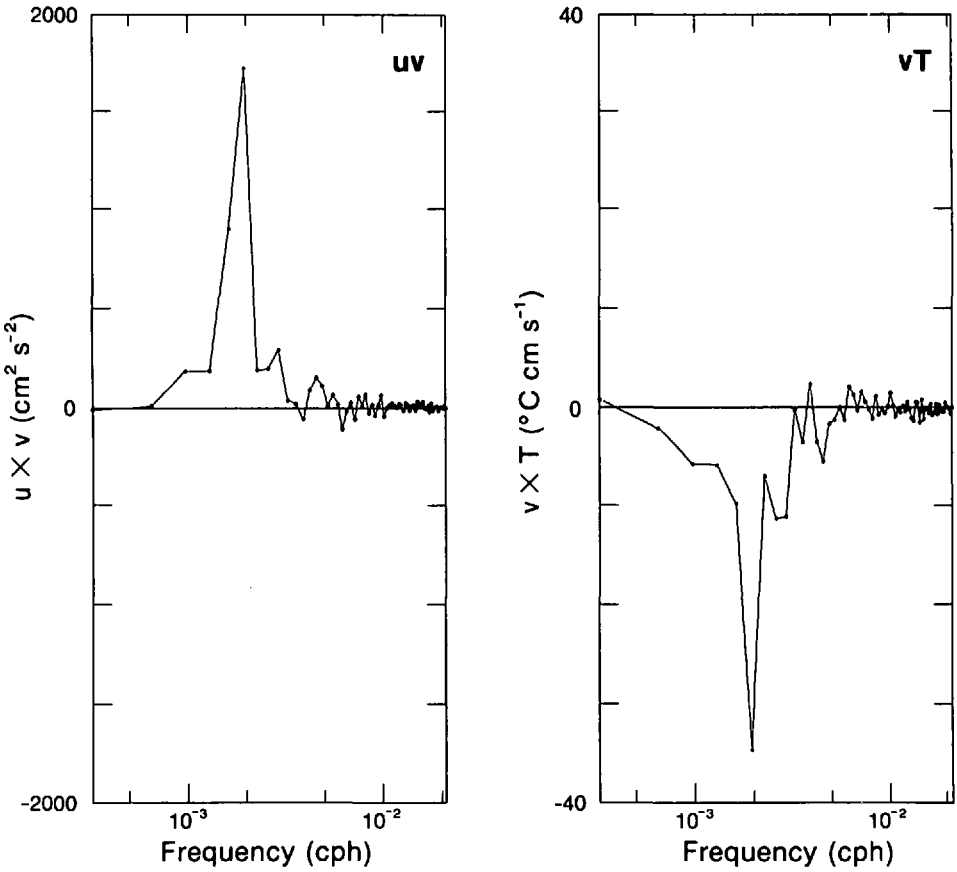

Figure 9. Cospectra between east velocity and north velocity (a) and between north velocity and temperature (b) for three 128-day pieces of the current meter records at 20 m depth on the north mooring at 110W. Covariance preserving plots are presented.

maximum of 700 $cm^2\ s^{-2}$ at the northern mooring at 110W; and their zonal velocity variance, $\overline{u'^2}$, is a factor of two smaller, exhibiting a maximum of order 1400 $cm^2\ s^{-2}$ versus the current meter maximum of 2700 $cm^2\ s^{-2}$. Such comparisons suggest that Hansen and Paul's mixture of spatial and temporal averaging may increase the eddy momentum flux values over purely temporal averages and their relatively small data base may cause some of the natural eddy variance to be contained in the mean flow variance. Analysis of the current meter measurements indicates that averaging time in excess of 400 days are generally necessary for statistically significant eddy fluxes, in contrast to Hansen and Paul's use of order 100 day records.

What is most notable is that the momentum flux divergence and heat flux convergence estimated from the current meter measurements agree reasonably well with Hansen and Paul's (1984) estimates from the drifting buoy trajectories. The

vertically integrated meridional divergence of the eddy momentum fluxes is 0.16 dyne cm^{-2} averaged between 152W and 110W, compared with their estimate of 0.3 dyne cm^{-2} averaged over 95W to 130W over the upper 50 m. The vertically integrated meridional eddy heat flux convergence is 245 ± 84 W m^{-2} which is somewhat larger than their estimate of 180 W m^{-2}. Both do agree within the estimated error. Thus, the eddy momentum flux divergence and heat flux convergence make substantial contributions to the zonal momentum and heat balances along the equator in the Pacific Ocean.

a. Eddy-induced circulation. Consideration of the eddy heat and momentum fluxes within the context of the Eliassen and Palm (1961) formulation provides a useful procedure for understanding how the substantial eddy fluxes measured here modify the mean flow. For example, the eddies, through the term $(-\partial/\partial y)\,\overline{v'T'}$, effect a large equatorward transport of heat. How the mean circulation accommodates such a large heat flux is an important question. In the Eliassen-Palm formulation, the eddy heat fluxes induce a mean vertical-meridional circulation which supplements the steady geostrophic circulation. For steady, zonally averaged flow in the absence of heating or cooling, the observed eddy heat flux convergence at the equator is balanced by a mean upward advection of colder water. The eddy-induced vertical velocity can be estimated to be $w_e = -(\partial/\partial y)(\overline{v'T'}/\theta_z)$. Since the zonally averaged eddy-induced circulation must be nondivergent, there is also an eddy-induced meridional velocity, $v_e = \partial/\partial z(\overline{v'T'}/\theta_z)$.

Values of $\overline{v'T'}/\theta_z$, contours of which represent the streamlines for the eddy-induced circulation, are strongly negative in the upper waters at the northern mooring at both 110W and 152W (Fig. 10). While it is difficult to smoothly contour these streamfunction values, the general pattern shows increasing values in a downward and southward direction implying a southward and upward eddy-induced circulation. Meridional velocities calculated from this streamfunction pattern are less than 1 cm s^{-1} and hence make only a small contribution to the measured meridional velocities (Fig. 3). The eddy-induced vertical velocities are upward at both 110W and 152W with a magnitude of order 0.5×10^{-3} cm s^{-1} (Fig. 11). They too are smaller than the upward velocities estimated from the horizontal divergence of the measured velocities in Figure 4b.

There are three different types of vertical velocity which need to be considered here. First, there is the observed or true vertical velocity which is best determined from the divergence of the measured velocity field (Fig. 4b). Second, there is the eddy-induced vertical velocity defined above in terms of a meridional divergence of the eddy heat fluxes. Third, there is the vertical velocity associated with the steady, geostrophic equatorial circulation which Bryden and Brady (1985) determined from a diagnostic model for this region of the equatorial Pacific.

For many situations, particularly in the atmosphere (Dunkerton, 1980), eddy effects drive nearly all of the observed zonally averaged vertical-meridional circulation. Those

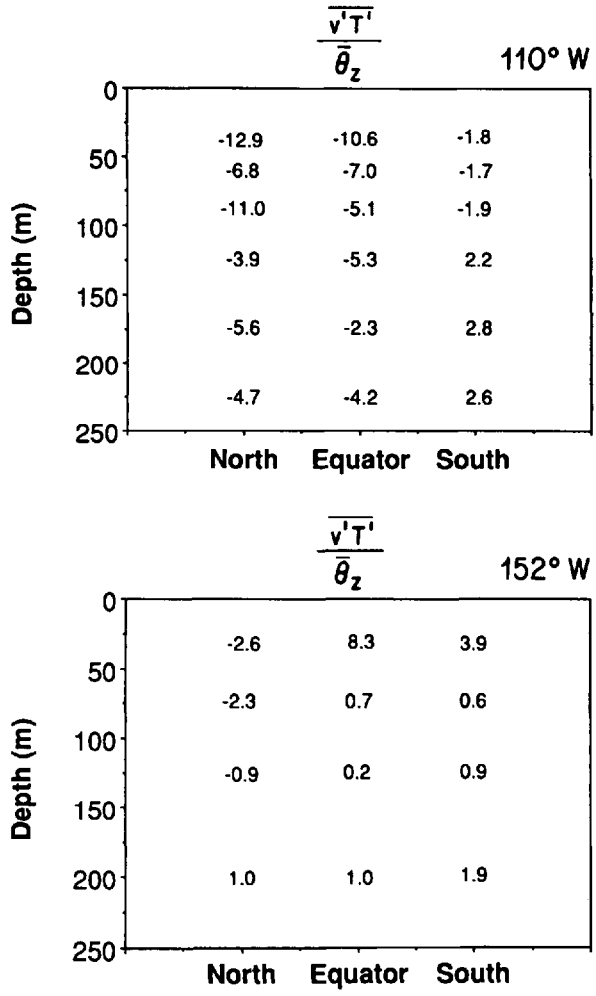

Figure 10. Streamfunction for the eddy-induced vertical-meridional circulation, $\overline{v'T'}/\bar{\theta}_z$, at 110W and at 152W.

situations led to the definition of the eddy-induced circulation and then to the study of the residual circulation, which is the difference between the observed and eddy-induced circulations and which is a small difference for those situations. For the equatorial ocean circulation observed here, however, the eddy-induced velocities are a factor of three or more smaller than the observed velocities; hence, the residual circulation is very similar in magnitude and direction to the observed circulation. Thus, the eddy-induced vertical velocity is not a useful approximation to the observed vertical velocity at the equator in the central Pacific Ocean.

In mid-latitudes, the vertical velocity associated with the geostrophic circulation is extremely small because the geostrophic constraints force the flow to be predominantly

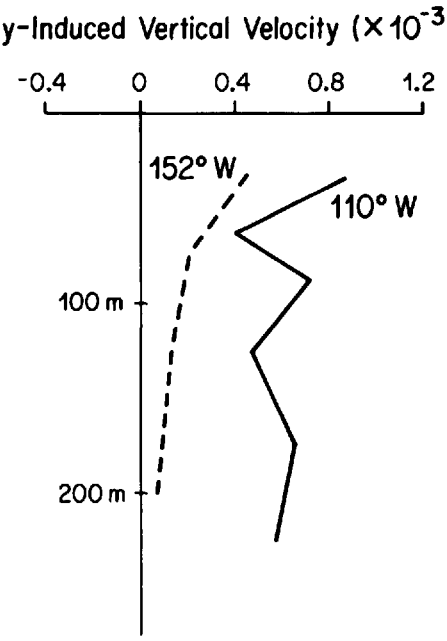

Figure 11. Eddy-induced vertical velocity at 110W and 152W.

horizontal. At the equator, the main geostrophic constraint on the size of the vertical velocity is absent. In fact, Bryden and Brady (1985) estimate vertical velocities as large as 2.9×10^{-3} cm s^{-1} associated with the geostrophic flow of the Equatorial Undercurrent eastward and upward along the sloping thermocline. Their geostrophic vertical velocities actually agree with the observed vertical velocities within measurement errors over the upper 150 m of the water column (Table 3). Thus, the steady, geostrophic vertical velocity, rather than the eddy-induced vertical velocity, accounts for most of the observed vertical velocity. The conclusion stressed by Bryden and Brady (1985) and elaborated by Brady and Bryden (1987) remains valid: the upwelling along

Table 3. Vertical velocity ($\times 10^{-3}$ cm s^{-1}).

Depth	Eddy-induced vertical velocity	Steady, geostrophic vertical velocity	Measured vertical velocity
32.5 m	0.7	1.5	2.2
75 m	0.4	2.7	3.6
125 m	0.3	1.4	3.0
200 m	0.3	−0.3	1.6
	$w_e = -(\partial/\partial_y)\,(v'T'/\theta_z)$	from Bryden and Brady (1985)	from Figure 4b

the equator is principally due to the eastward and upward flow of the Equatorial Undercurrent along the sloping isotherms.

The eddy-induced circulation may affect the zonal momentum balance for the mean flow. Including the advection of zonal momentum by the eddy-induced vertical-meridional circulation yields a zonal momentum balance where the total accelerative effect of the eddies is equal to the convergence of the Eliassen-Palm fluxes:

$$\frac{d\bar{U}}{dt} - f\bar{v} + \frac{\partial \bar{p}}{\rho_0 \partial x} - \frac{\partial \tau^x}{\partial z}$$
$$= -\frac{\partial}{\partial y}\left(\overline{u'v'} - \frac{\bar{U}_z}{\bar{\theta}_z}\overline{v'T'}\right) - \frac{\partial}{\partial z}\left(\overline{u'w'} - \frac{(f - U_y)}{\bar{\theta}_z}\overline{v'T'}\right) \equiv -\left(\frac{\partial}{\partial y}E^y + \frac{\partial}{\partial z}E^z\right) \quad (1)$$

where E^y and E^z are the meridional and vertical components of the Eliassen-Palm flux (Holton, 1983). For steady ($d/dt = 0$), zonally-averaged ($\partial/\partial_x = 0$) circulation on the equation ($f = 0$) in the absence of the forcing ($\partial\tau^x/\partial z = 0$), the convergence of the Eliassen-Palm flux must exactly equal zero. For equatorial circulation, this is the statement of the noninteraction theorem (Boyd, 1976; Andrews and McIntyre, 1976) in which the net effect of the eddies on the acceleration of the zonal flow is zero. For the equatorial ocean circulation where the zonal pressure gradient and zonal wind stress are the principal components in the zonal momentum balance (Mangum and Hayes, 1984), it is unlikely that such a noninteraction theorem would be valid. However, for their model of Kelvin wave interactions with zonal equatorial currents, McPhaden *et al.* (1986) found that the meridional component of the Eliassen-Palm flux was very small except near critical levels so that the wave momentum flux divergence, $(\partial/\partial y)$ $\overline{u'v'}$, was nearly everywhere compensated by the vertical advection by the eddy-induced circulation, $(\partial/\partial y)$ $(\bar{U}_z\overline{v'T'}/\bar{\theta}_z)$.

To determine whether the eddy momentum flux divergence is compensated by vertical advection by the eddy-induced circulation in the zonal momentum balance, values of $(\bar{U}_z/\bar{\theta}_z)$ $\overline{v'T'}$ are calculated at 152W and 110W and are found to be generally much smaller than values of $\overline{u'v'}$ at the northern and southern moorings but similar in magnitude to $\overline{u'v'}$ at the equatorial moorings. There is a tendency for the vertical advection by the eddy-induced circulation to partially balance the momentum flux at all moorings. Because the heat flux terms are relatively minor at the northern and southern moorings, however, the meridional derivative of the meridional Eliassen-Palm flux (Fig. 12) is similar in magnitude and vertical structure to the momentum flux divergence shown in Figure 6. The vertical integrals of the meridional derivative of the Eliassen-Palm flux at 152W and 110W are within 0.01 $cm^2\ s^{-2}$ of the integrals of the momentum flux divergence reported above. There is essentially no compensation of the eddy momentum flux divergence by the meridional divergence of the vertical advection by the eddy-induced circulation. Thus, after consideration of the Eliassen-Palm fluxes, the conclusion remains that the eddies act directly to decelerate the mean eastward flow by transporting eastward momentum meridionally from the equator.

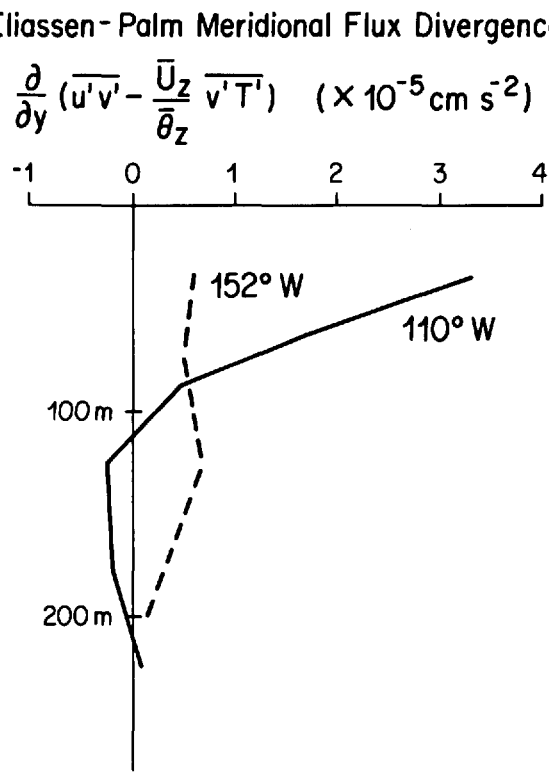

Figure 12. Profiles of the meridional derivative of the meridional component of the Eliassen-Palm flux $\partial/\partial y(\overline{u'v'} - (\bar{U}_z\overline{v'T'}/\bar{\theta}_z)$ at 152W and 110W.

Since the vertical momentum fluxes, $\overline{u'w'}$, remain inaccessible for direct estimation from moored current measurements, it is not possible to estimate the total vertical Eliassen-Palm flux. Calculations of the heat flux component of the vertical flux, $(f - \bar{U}y/\theta_z)\overline{v'T'}$, are made at 152W and 110W and both indicate that the effective eddy stress is smaller than 0.06 cm^2 s^{-2} throughout the water column, or an order of magnitude less than the zonal wind stress.

In summary, the eddy-induced vertical-meridional circulation is found to be an order of magnitude smaller than the observed circulation. In particular, the eddy-induced vertical velocity is much smaller than the steady, geostrophic upwelling associated with the eastward and upward flow of the Equatorial Undercurrent. Furthermore, meridional divergence of the eddy-induced vertical advection of zonal momentum is much smaller than the eddy momentum flux divergence in the zonal momentum balance. As shown above the eddies do have large, direct effects on the equatorial heat and zonal momentum budgets. Their indirect effects, however, in driving a vertical-meridional circulation and in modifying the zonal momentum balance are not the first order of importance.

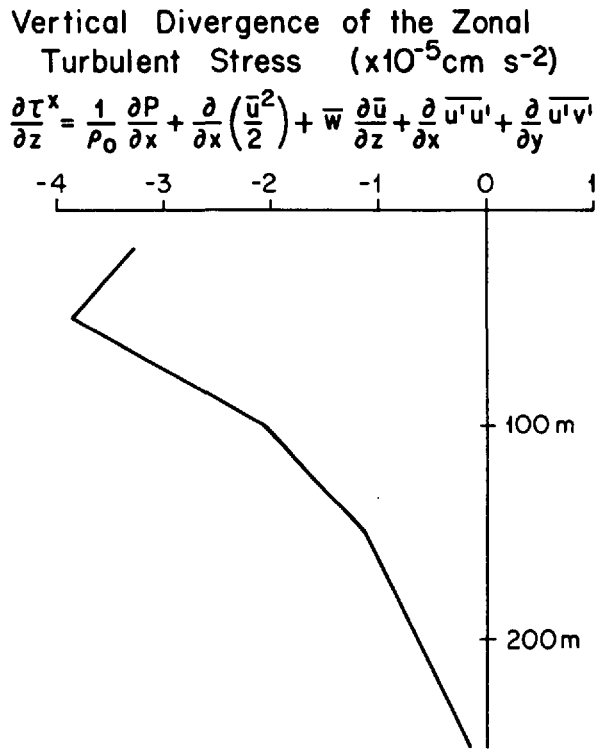

Figure 13. Profile of the vertical divergence of the zonal turbulent stress along the equator averaged over the region between 152W and 110W. The horizontal divergence of the eddy momentum fluxes in Figure 6 is combined with the estimates of zonal pressure gradient, zonal advection and vertical advection of zonal momentum by Bryden and Brady (1985) to derive this stress profile.

b. Profile of zonal stress. Because of the recent interest in the zonal momentum balance at the equator and particularly in the vertical profile of the zonal turbulent stress (Dillon *et al.*, 1989), it is worthwhile to make an indirect estimate of the vertical divergence of the zonal turbulent stress:

$$\rho_0 \frac{\partial}{\partial z}\tau^x = -\frac{\partial}{\partial z}\overline{u'w'} = \frac{1}{\rho_0}\frac{\partial \bar{p}}{\partial x} + \frac{\partial}{\partial x}\left(\frac{\bar{U}^2}{2}\right) + \bar{w}\frac{\partial \bar{U}}{\partial z} + \frac{\partial}{\partial x}\overline{u'u'} + \frac{\partial}{\partial y}\overline{u'v'}. \qquad (2)$$

The horizontal divergence of the eddy momentum fluxes in Figure 6 is combined with estimates of the zonal pressure gradient, zonal advection of zonal momentum and vertical advection of zonal momentum from Bryden and Brady's (1985) diagnostic model to derive a vertical profile of the vertical stress divergence (Fig. 13). All terms, eddy and mean, are estimated from data obtained over the same time period (1979 to 1981) and in the same NORPAX-EPOCS equatorial region (152W to 110W). Vertical integration of the right-hand side of (2) from 275 m depth to the surface yields

Table 4. High frequency momentum and heat flux divergences at 152W.

Depth (m)	$(\partial/\partial_y)\overline{u''v''}$ ($\times 10^{-5}$ cm s^{-2})	$(\partial/\partial_y)\overline{v''T''}$ ($\times 10^{-7}$°C s^{-1})
15	.01	−.03
50	−.04	.11
100	.09	−.70
150	.11	−.28
200	.02	−.04

an implied zonal wind stress of -0.47 dyne cm^{-2} which compares well with the climatological average wind stress calculated by Wyrtki and Meyers (1976) of -0.48 dyne cm^{-2}. More importantly, the profile indicates that the zonal turbulent stress divergence penetrates certainly below 100 m, much deeper than the order 30 m suggested by recent measurements of turbulent kinetic energy dissipation rates at the equator (Dillon *et al.*, 1988).

c. Comparison with eddy resolving numerical models. A primary motivation for this work was to determine whether the effects of eddies are adequately included in numerical simulations of equatorial circulation. Since the observations exhibit down-gradient eddy momentum fluxes above the core of the Equatorial Undercurrent but up-gradient fluxes beneath the core, models which parameterize eddy effects with single values for lateral eddy viscosity and diffusivity probably should not be expected to accommodate the observed eddy effects.

Philander and Pacanowski's (1980) use of constant eddy viscosity of 2×10^7 cm^2 s^{-1} and diffusivity of 1×10^7 cm^2 s^{-1} would appear to yield realistic eddy effects in the upper waters above the Undercurrent core. Below the Undercurrent, the model eddy effects are opposite to the observed effects. Philander and Pacanowski's model, however, is a hybrid in that monthly varying winds drive the model circulation but the model circulation resolves fluctuations of periods between a few days and a month if they arise by an instability mechanism. The model does exhibit fluctuations with periods of 15 to 60 days, whose heat and momentum fluxes compare favorably with the observed fluxes in the upper waters near 152W (Philander *et al.*, 1986). If the Philander and Pacanowski model realistically includes the 21-day fluctuations, the model viscosity and diffusivity then parameterize shorter time scale motions. In a further analysis of the 152W measurements, momentum and heat fluxes associated with fluctuations of periods shorter than one day were found to be an order of magnitude smaller than the low-frequency eddy fluxes in Figures 5 and 7. The high frequency momentum and heat flux divergences are also an order of magnitude smaller (Table 4) and hence the estimates of eddy viscosity and diffusivity are approximately 1×10^6 cm s^{-1} for the high frequency fluctuations as compared with 1×10^7 cm^2 s^{-1} for the low-frequency estimates in Tables 1 and 2. Thus, if the Philander and Pacanowski

model realistically portrays the fluctuations with periods between a few days and a few months and their effects on the equatorial circulation, it would seem that the model's lateral eddy viscosity and diffusivity coefficients need to be reduced by an order of magnitude to parameterize realistically the high frequency momentum and heat fluxes.

In the reduced gravity model of Busalacchi and O'Brien (1980), a small eddy viscosity of 1×10^6 cm^2 s^{-1} is purposely used so that eddy effects are only important for the model dynamics near the northern and southern model boundaries. Their model then ignores the eddy source of westward momentum along the equator which is of order 20% of the wind stress forcing their model circulation. Since Busalacchi and O'Brien's model effectively has no thermodynamic forcing nor any eddy diffusivity, it is hard to say whether it is the neglect of atmospheric heating or the neglect of eddy heat flux convergences that has more serious consequences for their model circulation.

Semtner and Holland's (1980) numerical model of equatorial circulation calculates eddy effects explicity by using a biharmonic mixing formulation for which is effective at very small scales only. They found that the model eddies transport eastward momentum away from the equator above the Undercurrent and eastward momentum toward the equator below the Undercurrent at about the same rates as found above in the current meter measurements. Their eddies appear to transport heat toward the equator at all depths, although their model has no bowling of isotherms below the Undercurrent so the deeper eddy heat fluxes are not necessarily up-gradient. Overall, Semtner and Holland's model appears to reflect the observed eddy effects more realistically than other existing equatorial models. It is unfortunate that this model has not been studied more thoroughly and extended as promised by Semtner and Holland (1980).

d. Future work. Because Philander's (1978) stability analysis and Cox's (1980) numerical model indicate that these 21-day oscillations originate north of the equator in the meridional shear of zonal velocity between the westward flowing South Equatorial Current and either the eastward flowing North Equatorial Countercurrent or the eastward flowing Equatorial Undercurrent, the moored array measurements are not well-suited for investigating the origin and effects of these oscillations. These array measurements are restricted too close to the equator to explore the instability mechanism in detail. Maximum momentum fluxes and heat fluxes do appear at the northern mooring; both are down-gradient in the near-surface waters as Cox's model indicates; and the resulting energy conversion (Brady, 1988) is dominated by the down-gradient momentum flux in agreement with both Philander's and Cox's analyses. The array measurements, however, do not extend far enough northward into the generation region.

To describe the energetic 21-day oscillations which appear to be primarily responsible for transporting zonal momentum away from the equator and heat toward the equator, moored array measurements extending at least from the equator to 8N where the maximum eastward velocity of the Countercurrent occurs and having zonal separations as large as 300 to 700 km will be necessary to estimate their zonal wavelength, sources of energy and mechanisms of momentum and heat transport. A key consideration in the design of such measurements must be to determine the vertical velocity associated with the 21-day oscillations and their vertical momentum flux, $\overline{u'w'}$. Brady (1988) inferred a vertical profile $\overline{u'w'}$ using a linear-wave temperature balance for a narrow frequency band containing periods from 37 to 14 days on a subset of the measurements at 110W and found that the vertical divergence of the vertical momentum flux led to an acceleration of the eastward flow above the core of the Undercurrent and a deceleration below the core. While these results are tentative, estimates of vertical velocity and vertical momentum flux are clearly needed in order to thoroughly understand the interaction between the 21-day oscillations and the mean equatorial circulation.

Array measurements extending farther away from the equator would also help to determine the extent of substantial eddy contributions to the momentum and heat balances in the equatorial region. Hansen and Paul's (1984) analysis indicates the large eddy momentum and heat flux divergences extend out to at least 5N and 5S. For example, their meridional heat flux convergence across 5N and 5S is still equivalent to a heating of the waters between 5N and 5S at an average rate of 45 W m^{-2} which is the same order of magnitude as the atmospheric heating of the equatorial zone. Current meter measurements both north and south of the equator are needed to substantiate statistically such large eddy effects with long data records and to determine their contributions to the dynamics and thermodynamics of the equatorial circulation.

Acknowledgments. The long time-series current meter measurements were obtained by Dr. David Halpern and Dr. Robert Knox with support from NOAA grant ERL8K2A2002 and NSF grants OCE78-26125 and OCE78-23134. The measurements were made at 110W as part of NOAA's Equatorial Pacific Ocean Climate Studies Program and at 152W as part of NSF's NORPAX Hawaii-to-Tahiti Shuttle Experiment. The analysis reported here was supported by the National Science Foundation under Grant OCE85-19551 as part of the Tropic Heat program. Dolores Chausse, Erika Francis, and Paul Freitag carried out the statistical calculations on the current meter records. Criticism of an earlier version by David Halpern, Phillip Richardson, George Veronis and two reviewers helped to improve the text. This is Woods Hole Oceanographic Institution Contribution number 6519.

REFERENCES

Andrews, D. G. and M. E. McIntyre. 1976. Planetary waves in horizontal and vertical shear: The generalized Eliassen-Palm relation and the mean zonal acceleration. J. Atmos. Sci., *33*, 2031–2048.

Boyd, J. P. 1976. The noninteraction of waves with the zonally averaged flow on a spherical

earth and the interrelationships of eddy fluxes of energy, heat and momentum. J. Atmos. Sci., *33,* 2285–2291.

Brady, E. C. 1988. Observations of equatorial 21-day wave-mean flow interaction at 110°W. M.I.T.-W.H.O.I. Joint Program Ph.D. thesis.

Brady E. C. and H. L. Bryden. 1987. Estimating vertical velocity on the equator. Oceanologica Acta, Special Volume, *6,* 33–38.

Bryden, H. L. and E. C. Brady. 1985. Diagnostic model of the three-dimensional circulation in the upper equatorial Pacific Ocean, J. Phys. Oceanogr, *15,* 1255–1273.

Busalacchi, A. J. and J. J. O'Brien. 1980. The seasonal variability in a model of the tropical Pacific. J. Phys. Oceanogr., *10,* 1929–1951.

Cox, M. D. 1980. Generation and propagation of 30-day waves in a numerical model of the Pacific. J. Phys. Oceanogr., *10,* 1168–1186.

Davis, R. 1976. Predictability of sea surface temperature and sea level pressure anomalies over the North Pacific Ocean, J. Phys. Oceanogr., *6,* 249–266.

Dillon, T. M., J. N. Moum, T. K. Chereskin and D. R. Caldwell. 1989. On the zonal momentum balance at the equator. J. Phys. Oceanogr. (in press).

Dunkerton, T. 1980. A Lagrangian mean theory of wave, mean-flow interaction with applications to nonacceleration and its breakdown. Rev. Geophys. Space Physics, *18,* 387–400.

Eliassen, A. and E. Palm. 1961. On the transfer of energy in stationary mountain waves. Geofysiske Publikasjoner, *22* (3), 1–23.

Eriksen, C. C., M. B. Blumenthal, S. P. Hayes and R. Ripa. 1983. Wind-generated equatorial Kelvin waves observed across the Pacific Ocean. J. Phys. Oceanogr., *13,* 1622–1640.

Halpern, D. 1980. A Pacific equatorial section from 172°E to 110°W during winter and spring 1979. Deep-Sea Res., *27,* 931–940.

—— 1987. Observations of annual and El Nino thermal and flow variations at 0°, 110°W and 0°, 95°W during 1980–85. J. Geophys. Res., *92,* 8197–8212.

Halpern, D., R. Knox and D. Luther. 1988. Observations of 20-day period meridional current oscillations in the upper ocean along the Pacific equator. J. Phys. Oceanogr., *18,* 1514–1534.

Hansen D. V. and C. A. Paul, 1984. Genesis and effects of long waves in the equatorial Pacific. J. Geophys. Res., *89,* 10431–10440.

Holton, J. R. 1983. The stratosphere and its links to the troposphere, *in* Large-Scale Dynamical Processes in the Atmosphere, B. Hoskins and R. Pearce, eds., Academic Press, New York, 227–303.

Knox, R. A., and D. Halpern. 1982. Long-range Kelvin wave propagation of transport variations in Pacific Ocean equatorial currents. J. Mar. Res., *40* (Suppl.), 329–339.

Lukas, R. 1987. Horizontal Reynolds stresses in the central equatorial Pacific, J. Geophys. Res., *92,* 9453–9463.

Mangum, L. J. and S. P. Hayes. 1984. The vertical structure of the zonal pressure gradient in the eastern equatorial Pacific. J. Geophys. Res., *89,* 10441–10449.

McPhaden, M. J., J. A. Prochl and L. M. Rothstein. 1986. The interaction of equatorial Kelvin waves with realistically sheared zonal currents, J. Phys. Oceanogr., *16,* 1499–1515.

Philander, S. G. H. 1978. Instabilities of zonal equatorial currents, 2. J. Geophys. Res., *83,* 3679–3682.

Philander, S. G. H., D. Halpern, D. Hansen, R. Legeckis, L. Miller, C. Paul, R. Watts, R. Weisberg and M. Wimbush. 1985. Long waves in the equatorial Pacific Ocean. Trans. Amer. Geophys. Un., *66,* 154.

Philander, S. G. H., W. J. Hurlin and R. C. Pacanowski. 1986. Properties of long equatorial waves in models of the seasonal cycle in the tropical Atlantic and Pacific Oceans. J. Geophys. Res., *91,* 14207–14211.

Philander, S. G. H. and R. C. Pacanowski. 1980. The generation of equatorial currents, J. Geophys. Res., *85*, 1123–1136.

Semtner, A. J., Jr. and W. R. Holland. 1980. Numerical simulation of equatorial ocean circulation. Part I: Basic case in turbulent equilibrium. J. Phys. Oceanogr., *10*, 667–693.

Wyrtki, K. 1974. Sea level and the seasonal fluctuations of the equatorial currents in the western Pacific Ocean. J. Phys. Oceanogr., *4*, 91–103.

Wyrtki K., and G. Meyers. 1976. The trade wind field over the Pacific Ocean. J. Applied Meteor., *15*, 698–704.

Received: *21 April, 1987;* revised: *18 October, 1988.*